PERGAMON

International Journal of Multiphase Flow 28 (2002) 1205–1222

International Journal of Multiphase Flow

www.elsevier.com/locate/ijmulflow

Finite element method simulation of turbulent wavy core–annular flows using a k–ω turbulence model method

T. Ko [a], H.G. Choi [b], R. Bai [a], D.D. Joseph [a,*]

[a] *Department of Aerospace Engineering and Mechanics, University of Minnesota, 110 Union Street S.E., Minneapolis, MN 55454, USA*

[b] *School of Mechanical and Aerospace Engineering, Seoul National University, Seoul 151-742, South Korea*

Received 12 February 2001; received in revised form 26 December 2001

Abstract

A numerical simulation of wavy core flow was carried out previously. They calculated the interfacial wave shape for laminar flow. In our present simulation, the shear stress transport turbulence model is used to solve the turbulent kinetic energy and dissipation rate equations and a splitting method is used to solve Navier–Stokes equations for the wave shape, pressure gradient and the profiles of velocity and pressure in turbulent wavy core flows. The wavelength decreases with Reynolds number $\Re$ and with the volume ratio η. The pressure gradient increases with Reynolds number $\Re$ and with the volume ratio η. High pressures are generated at a stagnation point leading to wave steepening, while low pressures are generated at a re-attachment point. The computed wave shapes and frictional losses are in satisfactory agreement with experiments and greatly improve on previous results. © 2002 Published by Elsevier Science Ltd.

Keywords: Shear stress transport; Interfacial wave shape; Numerical simulation

1. Introduction

Water lubricated pipelining is a method of transporting highly viscous fluids at low cost. A viscous fluid forms a core surrounded and lubricated by a water annulus. The water reduces the shear stress on the wall of the pipe. An important series of experiments on the water lubricated pipelining was carried out by Russell and Charles (1959); Russell et al. (1959), Charles (1963) and particularly by Charles et al. (1961). Glass (1961) and others found that the lowest pressure

* Corresponding author. Tel.: +1-612-626-8000; fax: +1-612-626-1558.
E-mail address: dept@aem.umn.edu (D.D. Joseph).

0301-9322/02/$ - see front matter
PII: S0301-9322(02)00024-1

gradient was achieved when the input ratio of water to oil was between 30% and 40%. Other experiments on water lubricated transportation in horizontal pipes were reported by Stein (1978) and Oliemans et al. (1985).

Ooms et al. (1984) and Oliemans and Ooms (1986) tried to use lubrication theory to analyze the case of a very viscous, wavy eccentric core–annular flow for laminar case. They showed that it generated a buoyant force proportional to the first power of the velocity to balance the gravity. In their study, the shape and amplitude of the wave must be given as empirical inputs. Oliemans et al. (1987) also tried to extend their results to the turbulent case but again the theory requires the inputs of waveforms and wavelengths, which are harder to identify in the turbulent flows. Their turbulence model underpredicts the variation of the pressure gradient with the velocity of core, even though wave amplitudes and wavelengths observed through their experiment are used as input data.

Bentwich (1964) studied for the laminar case with the basic core–annular model which the generators of the core and annulus are rigorously parallel and the cross-sections of the pipe and core are circular shaped, but the centers of them do not coincide. He solved the Poisson equation that governs in the eccentric core flow model with a Fourier series in bipolar coordinates. However, he did not use his solution to evaluate the friction factor or hold-up ratio. Huang et al. (1994) studied laminar and turbulent core–annular flow to assess the effects of eccentricity and the volume ratio on the friction factor and holdup ratio. They used a model of core–annular flow in which the oil core is a perfect cylinder with generators parallel to the pipe wall, but off-center and adopted a standard k–ε model with a low Reynolds number capability for turbulent case. Bai et al. (1996) achieved the important numerical calculation of the interfacial wave shape for laminar flow. The wavelength and amplitude were calculated by solving the normal stress balance on the interface of the wave. The developed waves are asymmetric with steep slopes near the high-pressure region at the front face of the wave crest and shallower slopes near the low-pressure region at the lee side of the crest.

In this paper, we extend the numerical simulation of axisymmetric laminar core–annular flow to turbulent case by adopting the shear stress transport (SST) k–ω model proposed by Menter (1994). The wavelength and amplitude are obtained by using the normal stress balance following Bai et al. (1996). A splitting method with linear equal-order finite element method proposed by Choi et al. (1997) is used as a solution algorithm and a consistent streamline upwind Petrov–Galerkin (SUPG) developed by Brooks and Hughes (1982) is adopted as a stabilizing technique for convection dominated flows. Using this code, the shape of interface, pressure distribution and secondary flow motions are analyzed for turbulent core–annular flow.

2. Governing equation

Consider two concentric immiscible fluids flowing down an infinite horizontal pipeline. We assume that the core is axisymmetric with interfacial waves that are periodic along the flow direction.

Patankar et al. (1977) decomposed the pressure in periodic fully developed flows as

$$P(x,r) = -\beta x + p(x,r), \tag{2.1}$$

where β is a mean pressure gradient and $p(x,r)$ represents the periodic part of the whole pressure P and behaves in periodic fashion from module to module. The term βx accommodates the general pressure drop along the flow direction.

The continuity equation and Navier–Stoke equation for the unsteady incompressible flow in cylindrical coordinates can be written as follows:

continuity equation

$$\frac{\partial}{\partial x}(\rho u)+\frac{1}{r}\frac{\partial}{\partial r}(r\rho v)=0, \tag{2.2}$$

x-momentum

$$\rho\left[\frac{\partial u}{\partial t}+u\frac{\partial u}{\partial x}+v\frac{\partial u}{\partial r}\right]=\beta-\frac{\partial p}{\partial x}+\frac{\partial}{\partial x}\left(\mu_{\text{eff}}\left(2\frac{\partial u}{\partial x}\right)\right)+\frac{1}{r}\frac{\partial}{\partial r}\left(r\mu_{\text{eff}}\left(\frac{\partial v}{\partial x}+\frac{\partial u}{\partial r}\right)\right)-\rho\frac{2}{3}\frac{\partial k}{\partial x}, \tag{2.3}$$

r-momentum

$$\rho\left[\frac{\partial v}{\partial t}+u\frac{\partial v}{\partial x}+v\frac{\partial v}{\partial r}\right]=-\frac{\partial p}{\partial r}+\frac{\partial}{\partial x}\left(\mu_{\text{eff}}\left(\frac{\partial v}{\partial x}+\frac{\partial u}{\partial r}\right)\right)+\frac{1}{r}\frac{\partial}{\partial r}\left(r\mu_{\text{eff}}\left(2\frac{\partial v}{\partial r}\right)\right)-2\mu_{\text{eff}}\frac{v}{r^2}-\rho\frac{2}{3}\frac{\partial k}{\partial x}. \tag{2.4}$$

The turbulent kinetic energy equation and the dissipation rate equation are obtained from Menter's shear stress transport model (Menter, 1994). The SST model utilizes the original k–ω model of Wilcox in the inner region of the boundary layer and switches to the standard k–ε model in the outer region of the boundary layer and in free shear flows. In the dissipation rate equation, the function F_1 is designed to be one in the near wall region (activating the original model) and zero away from the surface (activating the transformed model). Then the turbulent kinetic energy and the dissipation rate equation modified by SST model are written as

turbulent kinetic energy

$$\rho\left[\frac{\partial k}{\partial t}+u\frac{\partial k}{\partial x}+v\frac{\partial k}{\partial r}\right]=P_k+\frac{\partial}{\partial x}\left((\mu+\sigma_k\mu_T)\frac{\partial k}{\partial x}\right)+\frac{1}{r}\frac{\partial}{\partial r}\left(r(\mu+\sigma_k\mu_T)\frac{\partial k}{\partial r}\right)-\beta^*\rho k\omega, \tag{2.5}$$

dissipation rate equation

$$\rho\left[\frac{\partial \omega}{\partial t}+u\frac{\partial \omega}{\partial x}+v\frac{\partial \omega}{\partial r}\right]=\frac{\partial}{\partial x}\left((\mu+\sigma_\omega\mu_T)\frac{\partial \omega}{\partial x}\right)+\frac{\gamma}{v_t}P_k-\beta\rho\omega^2+\frac{1}{r}\frac{\partial}{\partial r}\left(r(\mu+\sigma_\omega\mu_T)\frac{\partial \omega}{\partial r}\right)+2(1-F_1)\rho\sigma_{\omega 2}\frac{1}{\omega}\frac{\partial k}{\partial x}\frac{\partial \omega}{\partial x}+2(1-F_1)\rho\sigma_{\omega 2}\frac{1}{\omega}\frac{\partial k}{\partial r}\frac{\partial \omega}{\partial r}, \tag{2.6}$$

where

$$P_k=\mu_T\left(2\left(\left(\frac{\partial u}{\partial x}\right)^2+\left(\frac{\partial v}{\partial r}\right)^2+\left(\frac{v}{r}\right)^2\right)+\left(\frac{\partial v}{\partial x}+\frac{\partial u}{\partial r}\right)^2\right),$$

$$\mu_{\text{eff}}=\mu+\mu_T.$$

Let ϕ_1 represent a constant in the original k–ω model ($\sigma_{k1},\ldots$), ϕ_2 a constant in the transformed k–ε model ($\sigma_{k2},\ldots$). The corresponding constant ϕ of the new model ($\sigma_k,\ldots$) is given as follows:

$$\Phi = F_1\Phi_1 + (1-F_1)\Phi_2. \tag{2.7}$$

All constants, as well as the function F_1, are given in Appendix A.

3. Numerical method

3.1. Four-step fractional method

The fully implicit four-step fractional finite element method (Choi et al., 1997) is used to integrate in time the continuity equation (2.2) and the momentum equations (2.3) and (2.4). In this approach, pressure is decoupled from those of convection, diffusion and other external forces. The fully implicit four-step fractional method is written as follows:

$$\rho\frac{\widehat{U}_i - U_i^n}{\Delta t} + \rho\frac{1}{2}\left(\widehat{U}_j\frac{\partial\widehat{U}_i}{\partial x_j} + U_j^n\frac{\partial U_i^n}{\partial x_j}\right) = -\frac{\partial p^n}{\partial x_i} + \frac{1}{2}\frac{\partial}{\partial x_j}\left(\hat{\tau}_{ij} + \tau_{ij}^n\right) + S_i^n, \tag{3.1}$$

$$\frac{U_i^* - \widehat{U}_i}{\Delta t} = \frac{1}{\rho}\frac{\partial p^n}{\partial x_i}, \tag{3.2}$$

$$\frac{\partial^2 p^{n+1}}{\partial x_i^2} = \frac{\rho}{\Delta t}\frac{\partial U_i^*}{\partial x_i}, \tag{3.3}$$

$$\frac{U_i^{n+1} - U_i^*}{\Delta t} = -\frac{1}{\rho}\frac{\partial p^{n+1}}{\partial x_i}, \tag{3.4}$$

where Δt is the time increment, $\widehat{U}_i$ and U_i^* are intermediate velocities, and superscript n denotes the time level. In the procedure, the intermediate velocity does not necessarily satisfy the continuity equation. At the first step, the intermediate $\widehat{U}_i$ is obtained by using velocities, pressure and external forces calculated on the previous time step. Hence, at the next step, the intermediate velocity is corrected by the pressure and the pressure is obtained from the continuity constraint.

The fact that the pressure is decoupled from the velocity in the fractional step method was utilized in the finite element analysis of the incompressible Navier–Stokes equations by several researchers, who proved that the fractional step method can be successfully applied to the finite element analysis. This approach is more accurate than the SIMPLE algorithm based finite element method for the same grid, because the fractional step method does not include any approximation procedure. This comparison is found in Choi et al. (1997).

3.2. Galerkin finite element discretization

The transport equations of momentum, turbulent kinetic energy and dissipation are discretized using a consistent streamline upwind Petrov–Galerkin method and the pressure equation using a Galerkin method. The weak formulations of the governing equation are derived by multiply them

by a corresponding weighting function and integrating over the spatial domain of a problem. The weak formulations of governing equation can be written as follows:

Find $U_i(x,t) \in H^1$, $k(x,t) \in H^1$ and $\omega(x,t) \in H^1$ such that

$$\int_\Omega \left[\rho w_i\left(\dot{U}_i + U_i\frac{\partial U_i}{\partial x_j} + \frac{1}{\rho}\frac{\partial p}{\partial x_i} - \frac{S_i}{\rho}\right) + \tau_{ij}\frac{\partial w_i}{\partial x_j}\right]\mathrm{d}\Omega - \int_{\Gamma_2} t_i w_i \,\mathrm{d}\Gamma_2 = 0$$
$$\forall w_i \in H^1,\ \ w_i|_{\Gamma_1} = 0,\ \ U_i|_{\Gamma_1} = b_i, \tag{3.5}$$

$$\int_\Omega \left[\rho w_k\left(\dot{k} + U_j\frac{\partial k}{\partial x_j} - \frac{1}{\rho}P_k + \beta^* k\omega\right) + \mu_k\frac{\partial k}{\partial x_j}\frac{\partial w_k}{\partial x_j}\right]\mathrm{d}\Omega - \int_{\Gamma_2} t_k w_k \,\mathrm{d}\Gamma_2 = 0$$
$$\forall w_k \in H^1,\ \ w_k|_{\Gamma_1} = 0,\ \ k|_{\Gamma_1} = b_k, \tag{3.6}$$

$$\int_\Omega \left[\rho w_\omega\left(\dot{\omega} + U_j\frac{\partial \omega}{\partial x_j} - \frac{\gamma}{\mu_T}P_k + \beta\omega^2 - 2(1-F_1)\sigma_{\omega^2}\frac{1}{\omega}\frac{\partial \omega}{\partial x_j}\frac{\partial k}{\partial x_j}\right) + \mu_\omega\frac{\partial \omega}{\partial x_j}\frac{\partial w_\omega}{\partial x_j}\right]\mathrm{d}\Omega$$
$$- \int_{\Gamma_2} t_\omega w_\omega \,\mathrm{d}\Gamma_2 = 0 \quad \forall w_\omega \in H^1,\ \ w_\omega|_{\Gamma_1} = 0,\ \ \omega|_{\Gamma_1} = b_\omega. \tag{3.7}$$

Considering that Galerkin method corresponds to a central finite difference formulation, a convection-dominated problem cannot be solved effectively without using a very dense grid. One of the methods to overcome this problem is the SUPG scheme in which the weighting function is different from the trial function. The SUPG formulation for momentum equation is stated as follows:

Find $U_i^h(x,t) \in H^h$ such that

$$\int_\Omega \left[\rho w_i^h\left(\dot{U}_i^h + U_j^h U_{i,j}^h + \frac{1}{\rho}p_{,i}^h - \frac{S_i}{\rho}\right) + \tau_{ij}^h w_{i,j}^h\right]\mathrm{d}\Omega - \int_{\Gamma_2} t_i^h w_i^h \,\mathrm{d}\Gamma_2$$
$$+ \sum_{e=1}^{N_e}\int_{\Omega_e} \tilde{p}_i^h \rho\left(\dot{U}_i^h + U_j^h U_{i,j}^h + \frac{1}{\rho}p_{,i}^h - \tau_{ij,j}^h - \frac{S_i}{\rho}\right)\mathrm{d}\Omega = 0,$$
$$\forall w_i^h \in H^h,\ \ w_i^h\big|_{\Gamma_1} = 0,\ \ U_i^h\big|_{\Gamma_1} = b_i, \tag{3.8}$$

where $\tilde{p}_i^h = c_j w_{i,j}^h$ is a perturbation weighting function. This is derived from a tensorial artificial diffusion in a multidimensional space which acts along the flow direction. In the present study, the pertubation weighting function is applied to all terms in the momentum equation by the consistent SUPG method. The coefficients of the pertubation weighting function are given in Appendix B.

The Poisson type pressure equation is obtained from the continuity constraint. Using the divergence theorem, the weak formulation of continuity equation can be expressed as follows:

$$\int_\Omega w_{,i} U_i^{n+1}\,\mathrm{d}\Omega = \int_\Gamma w U_i^{n+1} n_i \,\mathrm{d}\Gamma. \tag{3.9}$$

Then, inserting Eq. (3.4) into the left-hand side of Eq. (3.9), the following Poisson type pressure equation is obtained as follows:

$$\frac{\Delta t}{\rho}\int_\Omega w_{,i} p_{,i}^{n+1}\,\mathrm{d}\Omega = \int_\Omega w_{,i} U_i^*\,\mathrm{d}\Omega - \int_\Gamma w U_i^{n+1} n_i \,\mathrm{d}\Gamma. \tag{3.10}$$

When used with a fractional four-step method, the pressure equation (3.10) has an advantage in treating the outflow boundary condition, because the unknown U_i^{n+1} is well approximated by the known $\widehat{U}_i$ through Eqs. (3.2) and (3.4).

The solution at steady state is sought through time marching of the corresponding unsteady governing equation. Therefore, the value of $1/\Delta t$ can be considered as an inertial relaxation factor of steady SIMPLE algorithm (Patankar, 1980).

3.3. Calculation of the interfacial wave shape

For wavy core–annular flow simulations with highly viscous fluids, the viscosity of the core liquid is much greater than that of annular liquid. The flow of oil can be regarded as a creeping motion on the forward motion of a rigid core. The slow secondary motion should not have a great effect on the overall dynamics. Therefore, the core flow is assumed to be solid with standing waves on the interface.

The normal stress equilibrium condition on the interface is written as follows:

$$(-\|P\| + 2H\sigma) + \boldsymbol{n} \cdot \|2\mu D\| \cdot \boldsymbol{n} = 0, \tag{3.11}$$

and the shear stress equilibrium condition is written as follows:

$$\boldsymbol{t} \cdot \|2\mu D\| \cdot \boldsymbol{n} = 0, \tag{3.12}$$

where $D = (1/2)(\nabla U + \nabla U^T)$, $\|\cdot\| = (\cdot)_1 - (\cdot)_2$, the subscript 1 and 2 indicate the core and annulus respectively, $2H$ is the sum of the principal curvature, σ is the coefficient of interfacial tension, $\boldsymbol{n} = \boldsymbol{n}_{12}$ is the unit normal vector from liquid 1 to 2 and $\boldsymbol{t}$ is the unit tangent vector.

The viscous part of the normal stress condition Eq. (3.11) on the interface vanishes

$$\boldsymbol{n} \cdot \|2\mu D\| \cdot \boldsymbol{n} = 2\mu_1 \frac{\partial U_{n1}}{\partial n} - 2\mu_2 \frac{\partial U_{n2}}{\partial n} = 0, \tag{3.13}$$

since

$$\frac{\partial U_s}{\partial s} + \frac{\partial U_n}{\partial n} = 0, \tag{3.14}$$

and on the interface

$$\frac{\partial U_s}{\partial s} = 0. \tag{3.15}$$

Therefore, the normal stress condition on the interface can be rewritten as follows:

$$\|P\| = 2H\sigma. \tag{3.16}$$

The periodic pressure equation (2.1) is rewritten for each core and annulus as follows:

$$P_1 = -\beta x + C_{p1}, \tag{3.17}$$

$$P_2 = -\beta x + p(x, y) + C_{p2}, \tag{3.18}$$

where C_{pi} is constant. Hence, the normal stress balance at the interface Eq. (3.16) is expressed in Bai et al. (1996) as follows:

$$\frac{\sigma}{f\left(1+\left(\frac{\mathrm{d}f}{\mathrm{d}x}\right)^2\right)^{1/2}}-\frac{\sigma\frac{\mathrm{d}^2f}{\mathrm{d}x^2}}{\left(1+\left(\frac{\mathrm{d}f}{\mathrm{d}x}\right)^2\right)^{3/2}}=\|P\|=P_1-P_2, \tag{3.19}$$

where $f = f(x)$ is the height of interface from center line.

In order to solve our wavy core–annular problem for a given wave speed, we must compute β. the pressure drop in one wave is define as βL, where L is length of one wave. The βL may be expressed by the shear stress acting on the wall as follows:

$$\beta LA = F_x = 2\pi R\int_0^L \tau_{\mathrm{w}}\,\mathrm{d}x, \tag{3.20}$$

where A is the area of the cross-section of pipe.

4. Numerical results

4.1. Validation of turbulent code

4.1.1. The fully developed pipe flow

To verify the present turbulent code, fully developed Poiseuille flow in pipe is calculated at various Reynolds numbers 200–40,000. The Reynolds number is defined as $Re = \rho UD/\mu$, where U is the mean velocity and D is the diameter of the pipe. The length of calculation domain is long enough to get the fully developed profile for the velocity, pressure and kinetic energy. The boundary conditions at solid surfaces are given as follows:

$$u = v = k = 0, \quad \omega = \frac{6v}{\beta_1(\Delta y_1)^2}, \tag{4.1}$$

where Δy_1 is the distance to the next grid point away from the wall. The Neumann boundary condition $\partial u/\partial x = \partial k/\partial x = \partial\omega/\partial x = 0$ is applied for u, k and ω and the Dirichlet boundary condition $v = 0$ is applied at exit. The boundary conditions at inlet are given as follows:

$$u = U_{\mathrm{in}}, \quad v = 0, \quad \omega = \frac{U_{\mathrm{in}}}{L}, \quad v_t = 10^{-2}v, \quad k = v_t\omega. \tag{4.2}$$

The friction factor is computed for various Reynolds numbers from 200–40,000 in the fully developed pipe flow and shown on Fig. 1. Note that the present numerical method gives accurate results for the turbulent flow as well as for the laminar flow. For laminar flow, the computed results of friction factor satisfy the Hagen–Poiseuille equation $\lambda = 64/Re$. The results of turbulent friction factor are represented by Blasius' correlation $\lambda = 0.316/Re^{0.25}$.

Fig. 2(a) and (b) shows the velocity profile and the profile of turbulent kinetic energy of a fully developed pipe flow for $Re = 40{,}000$. The results obtained from the present turbulent code are compared with the results of Wilcox's original k–ω model and the experimental data of Laufer (1952) for Reynolds number based on pipe diameter and average velocity of 40,000.

From the comparison with the result of Wilcox's k–ω model and experimental data for the velocity profile and the turbulent kinetic energy profile, we can see that that the present code using

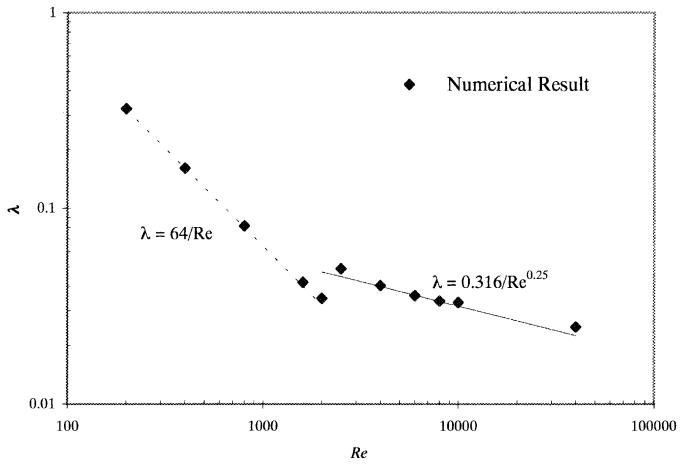

Fig. 1. The friction factor vs. Reynolds number in the fully developed pipe flow. (– – –) Hagen–Poiseuille equation for laminar flow; (—) Blasius' correlation for turbulent flow.

the Menter's SST model and the SUPG method gives more accurate result than the original k–ω model in fully developed pipe flow. The profiles obtained from our simulation at region away from the wall have more accurate values than near the wall.

4.1.2. The wavy core–annular flow

With the assumptions and equations described in Section 3.3, the wave shape of core flow and the profile of annular flow are computed for given wave speed c, water flow rate Q_w and average oil radius R_1. In our present simulation, the wall moves with core velocity c opposite the core; in this frame the core is standing. Then, we calculate the flow profiles in the annular region. The boundary conditions at wall are given as follows:

$$u = c, \quad v = k = 0, \quad \omega = \frac{6v}{\beta_1(\Delta y_1)^2} \tag{4.3}$$

and the ones at the interface are given as a stationary solid boundary condition Eq. (4.1).

Before the flow field in the annulus is calculated, we assume a free surface shape around a given average core radius R_1. During each iteration of the flow field, the pressure gradient β is adjusted to satisfy the force balance in one wavelength. Using the pressure on the surface obtained at the previous step, the shape of surface is calculated by solving the normal stress condition Eq. (3.19). The wavelength is adjusted in every iteration in order to get a converging surface shape for the given average core radius R_1 and water flow rate Q_w. The new interface determined at the previous step is used in computing the flow field again. Then, these steps are repeated until the solutions are converged.

The mesh and boundary conditions for the velocity are shown in Fig. 3. We define the Reynolds number as (see Arney et al. (1993) for a discussion of $\Re$)

$$\Re = \frac{\rho VD}{\mu}\left[1 + \eta^4(m-1)\right] = Re\left[1 + \eta^4(m-1)\right], \tag{4.4}$$

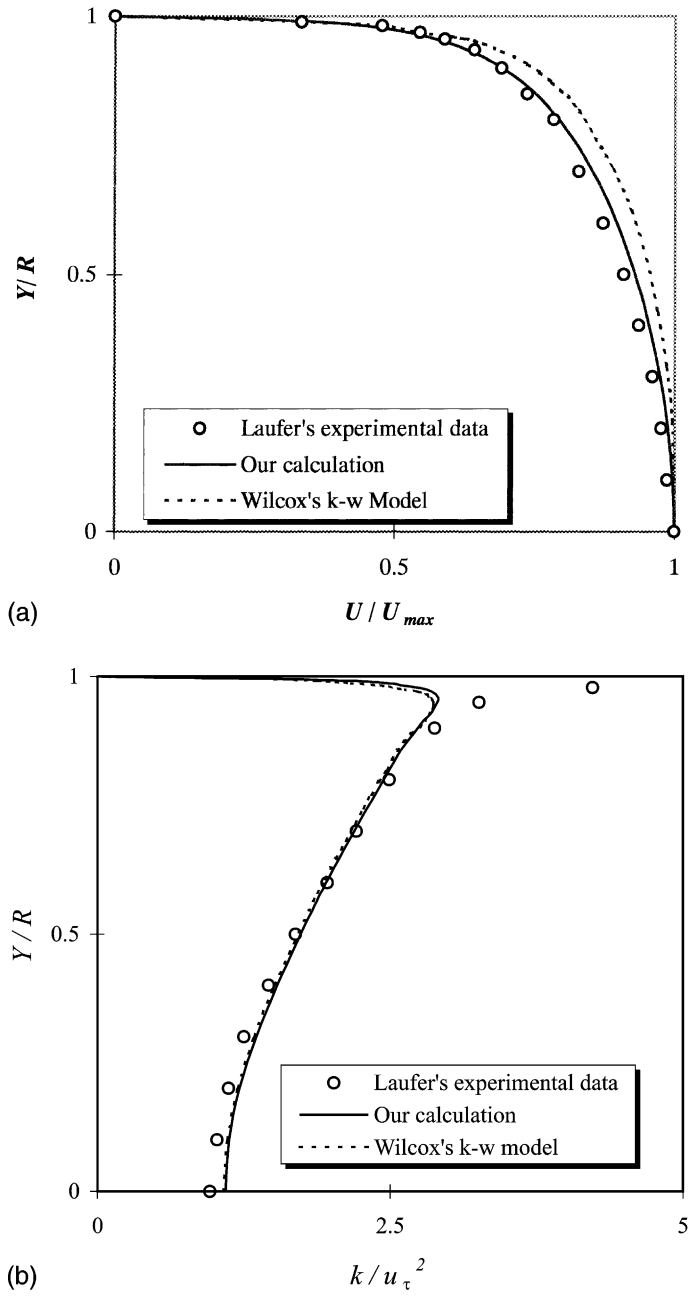

Fig. 2. (a). The comparison of computed and measured velocity profile in the turbulent pipe flow at $Re = 40{,}000$. Our result is closer to the experimental data than Wilcox's k–ω model, particularly in the region away from the wall. (b) Comparison of computed and measured profile of turbulent kinetic energy in the turbulent pipe flow at $Re = 40{,}000$. R is a radius of pipe and $u_\tau = \sqrt{\tau_w/\rho}$.

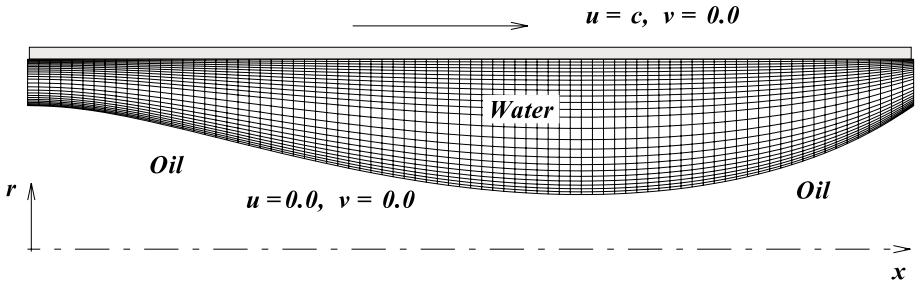

Fig. 3. The mesh of calculation domain has the body fitted and structured mesh and the boundary conditions at the wall and interface are given as the solid boundary condition. The wall moves with corevelocity c and the core is standing.

where $V = (Q_1 + Q_2)/\pi R_2^2$ is the mean velocity, $\eta^2 = R_1^2/R_2^2$ is the core fraction and $m = \mu_2/\mu_1$ is the viscosity ratio.

Fig. 4 shows the velocity profile in the annulus for laminar flow and turbulent flow. When the wall moves and the flow is driven by pressure, the velocity profile on the crest of wave for $\Re = 6700$ (Fig. 4 (b)) has the typical S-shape expected for turbulent Couette flow. For $\Re = 1000$ (Fig. 4(a)), the profile has the full shape expected for laminar Couette flow with a positive pressure gradient.

Here, we introduce the hold-up ratio as a dimensionless parameter for core–annular flow. The hold-up ratio h is defined as the ratio Q_1/Q_2 of volume flow rate to the ratio V_1/V_2 of volume in the pipe

$$h = \frac{Q_1/Q_2}{V_1/V_2} = \frac{Q_1/Q_2}{R_1^2/(R_2^2 - R_1^2)} = \frac{c}{c_2}, \tag{4.5}$$

where $c = Q_1/\pi R_1^2$ is the wave speed for rigid core flow and $c_2 = Q_2/\pi(R_2^2 - R_1^2)$ is the average velocity of annular flow. The dimensionless input parameters $\Re$, h and η replace the dimensional input parameters Q_w, c and R_1 in the present simulation. The definition of the dimensionless parameters L^*, p^* and β^* are defined as follows:

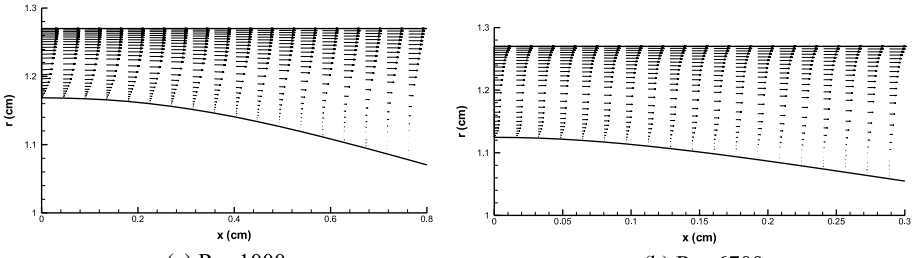

(a) R = 1000 (b) R = 6700

Fig. 4. The comparison of the velocity profile of annular flow for laminar flow ($\Re = 1000$) and turbulent flow ($\Re = 6700$).

$$L^* \text{ is dimensionless wavelength} = L/R, \tag{4.6}$$

$$\beta^* \text{ is dimensionless pressure gradient} = \frac{\beta \rho R_2^2}{\mu^2}, \tag{4.7}$$

$$p^* = \{p(f(x),x) - P_2(f(L),L)\}\frac{\rho R_p^2}{\mu^2}. \tag{4.8}$$

To validate the present code for core–annular flow, our result for laminar code using the finite element method is compared with the result from Bai et al. (1996) based on the finite difference method. The wavelength and pressure gradient is calculated for the case with $h = 1.4$ and $\eta = 0.8$. To compare the wavelength and pressure gradient obtained by solving the turbulent equations for high Reynolds number with results obtained from the typical direct numerical simulation without using any turbulent model, the simulations are done by two approaches with same grid points.

Figs. 5 and 6 show how the wavelength and the pressure gradient vary with $\Re$ for fixed $h = 1.4$ and $\eta = 0.8$. The wavelength decreases with $\Re$ and the pressure gradient increases with $\Re$ for fixed h and η. From these figures, we can note that, for high Reynolds numbers, the results obtained from the turbulent two-equation model (dotted line) differ greatly from a direct numerical simulation of laminar flow using same grid points. For higher Reynolds numbers, the wavelength is shorter and the pressure gradient is larger for the turbulent code than for the laminar code. The present laminar code gives results close to the data from Bai et al. (1996).

Table 1 compares the computed value of the wavelength with measured data from experiments for various $\Re$ and a fixed $h = 1.4$ and $\eta = 0.826$. It is apparent that the turbulent code gives more accurate results at high Reynolds numbers. In the experiment for horizontal wavy core flow, the input is Q_1 and Q_2 and the values of $\Re$, h and η for various Q_1 and Q_2 are obtained from image

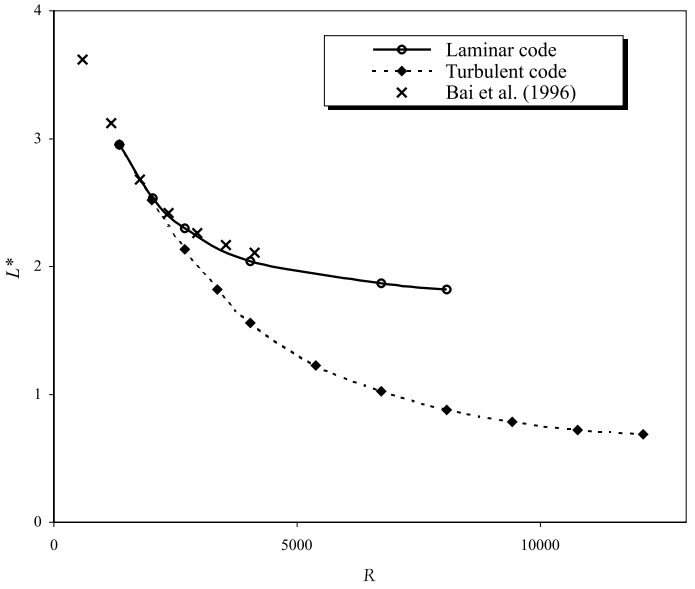

Fig. 5. The dimensionless wavelength L^* vs. Reynolds number $\Re$ at $h = 1.4$ and $\eta = 0.8$.

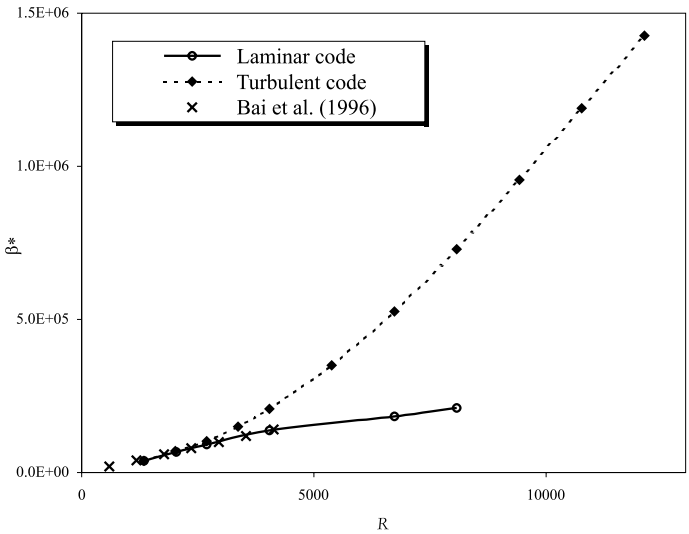

Fig. 6. The dimensionless pressure gradient β^* vs. Reynoldsnumber $\Re$ at $h = 1.4$ and $\eta = 0.8$.

Table 1
Comparison of the measured values of the wavelength with measured at $h = 1.4$ and $\eta = 0.826$

	Reynolds number				
	4000.2	4684.6	5333.6	5811.5	8000.4
Dimensionless wavelength (L^*)					
Experiments	1.35786	1.23102	1.07574	1.02346	0.82907
Laminar code	1.91	1.83	1.76	1.72	1.6
Turbulent code	1.55	1.34	1.2	1.11	0.9
Error (%)					
Laminar code	28.9078	32.7311	38.8784	40.4963	48.1828
Turbulent code	12.3961	8.13281	10.355	7.79613	7.88061

processing and Eq. (4.5). The movies of core–annular flow are recorded by using a Kodak Ekta-Pro EM high-speed video camera that takes at rate up 1000 frames per second. The movies are played and analyzed frame by frame with a computer.

Even though the computed values from turbulent code and measured values of the wavelength are not the same, we can see the same trend in both; the wavelength is a decreasing function of $\Re$. The values obtained from the computation using the turbulent model are closer to the values of experiment than the values from the laminar models. While the error for laminar code increases to around 50% for higher Reynolds number, the error for the turbulent code decreases to less than 8%. We can infer that the error comes from the assumptions as rigid core and axi-symmetric core flow with zero density difference between core and annulus. In the experimental measurement, the core is slightly lighter than the annulus and has a limited viscosity even if it is so larger than one of water. Therefore, the core flow is off-center and deformable.

4.2. Numerical results

We study how the wavelength, pressure gradient, pressure distribution on the interface and wave shape vary with $\Re$ and η. In the vertical pipeline studied in the experiment of Bai et al. (1992), the hold-up ratio is about 1.39 independent of the input flow rate Q_1 and Q_2. In the numerical simulation of the wavy core flow for laminar flow by Bai et al. (1996), they computed many results for $h = 1.4$. We also compute for fixed $h = 1.4$ to compare our results with theirs. In our computation, we choose the actual physical parameter in wavy core flow of water in a one inch diameter pipe, $\mu_2 = 0.01$ poise, $\rho = 1$ g/cm^3 and $\sigma = 26$ dyne/cm.

Fig. 7 shows the secondary motions and pressure distribution for $\Re = 1000$ and 5000. The flow in the annulus is composed of a straight flow and an eddy. The low pressure at the back of the crest of wave is associated with the reattachment point, the high pressure at the front of the crest of wave is related to a stagnation point. We note that the area of the eddy for turbulent flow is smaller than for laminar flow due to increasing of the momentum transfer from main flow in turbulent flow.

Fig. 8 shows the wavelength and the wave shape for various values of $\Re$ at $h = 1.4$ and $\eta = 0.8$. When the Reynolds number increases, the wave steepens at the front of the crest and the wavelength is decreased.

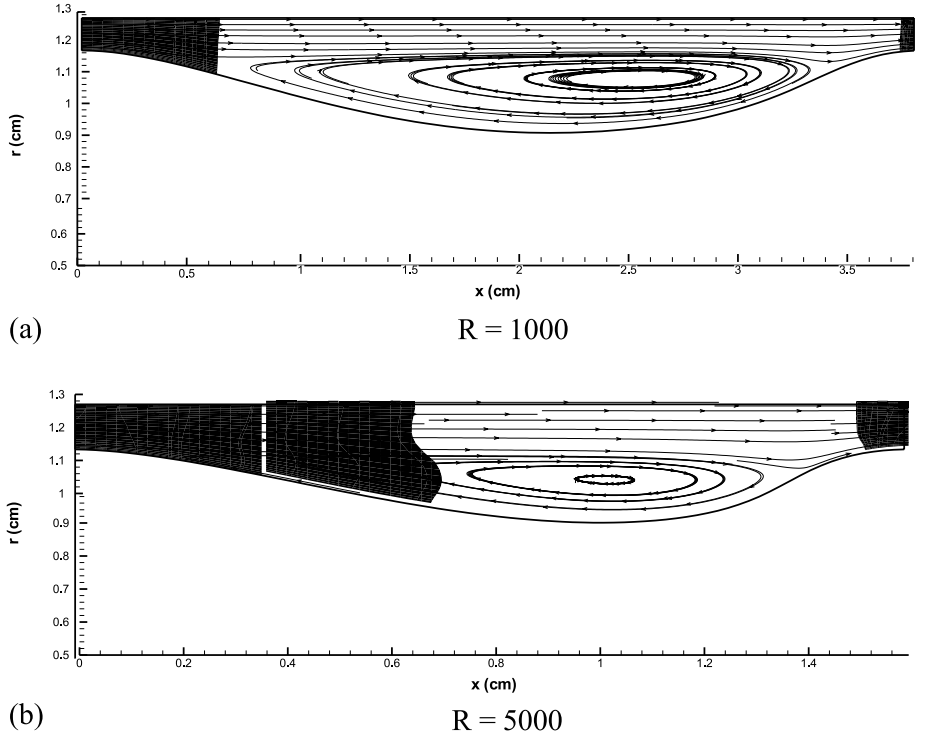

Fig. 7. The comparison of the pressure profile and streamline ofannular flow for laminar flow ($\Re = 1000$) and turbulent flow ($\Re = 5000$). The dark color indicates a low pressure and the light one indicates a high pressure.

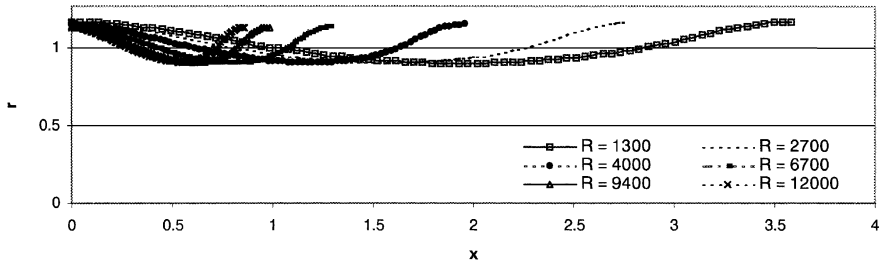

Fig. 8. The wave shape for different Reynolds numbers at $h = 1.4$ and $\eta = 0.8$.

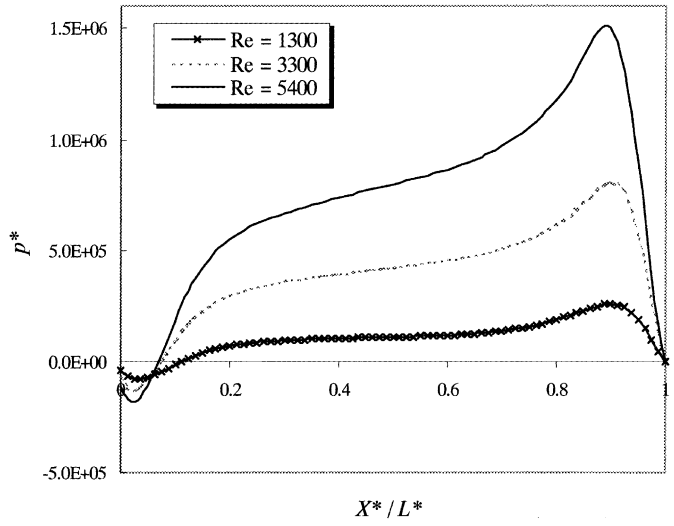

Fig. 9. The dimensionless pressure on the interface at $\Re = 1300$, 3300 and 5400. The holdup ratio h is fixed at 1.4 and the volume ratio η is fixed at 0.8.

Figs. 5 and 6 show how the wavelength and the pressure gradient vary with $\Re$ for any fixed hold-up ratio and volume ratio. Fig. 9 shows the pressure distribution on the oil–water interface. The positive pressure peak appears at the stagnation point and the negative pressure peak at the reattachment point. For $0.3 < x^*/L^* < 0.7$, the pressure on the interface increases with $\Re$ for high $\Re$ while for low $\Re$ the pressure does not change.

Fig. 10 shows how the wavelength and pressure gradient vary with η for fixed $h = 1.49$ and $c = 25$ cm/s. Note that the wavelength decreases with η and the pressure gradient increases with η.

To validate the turbulent code for core–annular turbulent pipe flow, the pressure gradient β for various diameters of pipe was computed and compared with the Blasius' formula for turbulent pipe flow. From the relationship between the pressure gradient β and the shear stress τ_w on the pipe walls, Joseph et al. (1998) obtained an expression for the pressure gradient β (kPa m^{-1}), in terms of the 7/4th power of the velocity U (m s^{-1}) to the 5/4th power of the pipe radius R_0 (m), namely

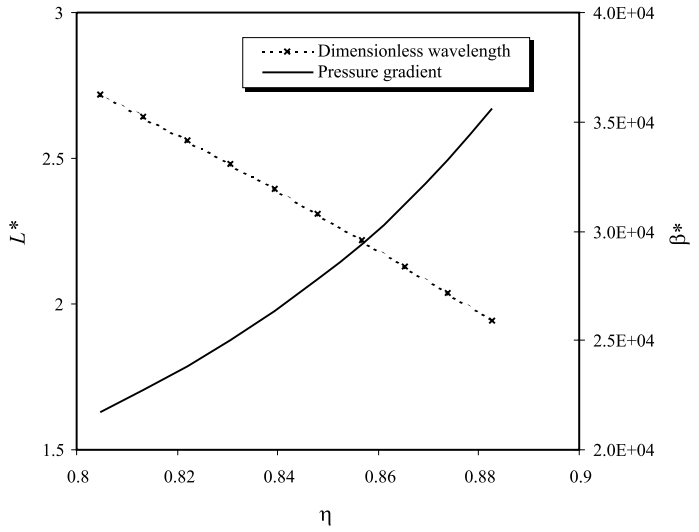

Fig. 10. The dimensionless wavelength L^* and pressure gradient β vs. η at $h = 1.49$ and the wave speed $c = 25$ cm/s.

$$\beta = K\frac{U^{7/4}}{R_0^{5/4}} = k\left\{\frac{\rho^3\mu}{2^9}\right\}^{1/4}\frac{U^{7/4}}{R_0^{5/4}}. \tag{4.9}$$

where k is an unknown constant ($k = 0.316$ for water alone).

In our simulation, pipe radius R_0 is replaced by R_2 and velocity U by the mean velocity V. These curves for various pipe radius (0.25′, 0.5′ and 1′) are shown in Fig. 11. These curves collapse to a single curve with the value $k = 0.317$ which is almost same with the Blasius value for water alone ($k = 0.316$). From this result, we can write the relation of the pressure gradient for core–annular flow with an infinitely viscous core and for water alone flow as follows:

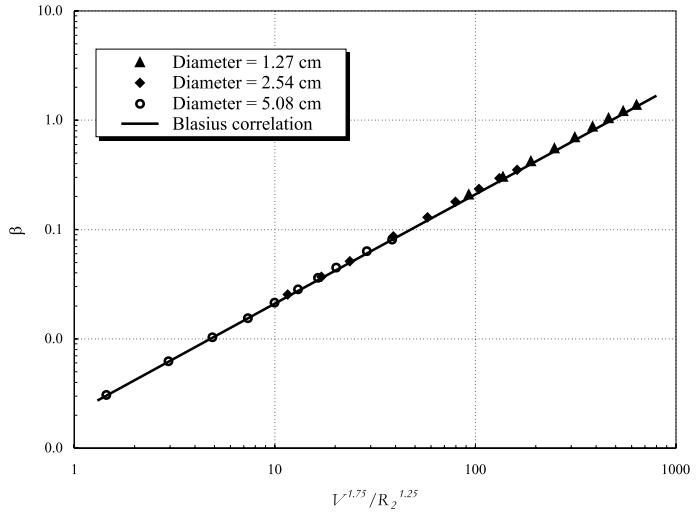

Fig. 11. The pressure gradient β vs. $V^{1.75}/R_2^{1.25}$ for various pipe radius at the core–annular turbulent pipe flow.

$$\beta_{\text{CAF with rigid core}} = 1.01\beta_{\text{water alone}} \tag{4.10}$$

The pressure gradients for experimental core–annular flow with deformable core is bigger than calculated pressure gradient with rigid core. It can be said that wavy core flow of an infinitely viscous core in turbulent water can be transported as cheaply as water alone. Increased costs due to secondary motions in the viscous core and to fouling of the pipe wall are presently under study.

5. Conclusion

- The present code using the shear stress transport model and the streamline upwind Petrov–Galerkin method gives more accurate results than the original k–ω model in fully developed turbulent pipe flow.
- For the turbulent wavy core–annular flow with fixed hold-up ratio and volume ratio, the wavelength obtained from the turbulent code is closer than the laminar code to the values of experiment. The pressure gradient in turbulent flow increases more sharply with Reynolds number than the pressure gradient computed with the laminar code.
- For the turbulent core–annular flow, the area of the eddy in the annulus is smaller than for the laminar flow due to increasing of the momentum transfer from main flow. The wave steepens more at the front of the crest and the wavelength decreases more than in laminar flow.
- While the wavelength decreases with Reynolds number at fixed hold-up ratio and volume ratio, and the wavelength decreases with volume ratio at fixed hold-up ratio and the wave speed, the pressure gradient has an opposite trend for the same cases.
- The pressure gradient calculated from turbulent code satisfies with Blasius' formula in the turbulent core–annular flow with a rigid core; the pressure gradient is a linear function of the 7/4th power of the mean velocity to the 5/4th power of the pipe radius and the constant k is close to the value for water alone turbulent pipe flow.

Acknowledgements

This work was supported by the DOE (Engineering Research Program of the Department of Basic Energy Sciences), the NSF/CTS under Grant Opportunities for Academic Liasons with Industry and the Minnesota Supercomputer Institute.

Appendix A. The coefficients of shear-stress transport model

The constants of set 1 (ϕ_1) are

$$\sigma_{k1} = 0.85,\ \sigma_{w1} = 0.5,\ \beta_1 = 0.075,\ a_1 = 0.31,\ \kappa = 0.41,\\ \gamma_1 = \beta_1/\beta^* - \sigma_{\omega 1}\kappa^2/\sqrt{\beta^*}. \tag{A.1}$$

The constants of set 2 (ϕ_2) are

$$\sigma_{k2} = 1.0,\ \sigma_{w2} = 1.856,\ \beta_2 = 0.0828,\ \beta^* = 0.09,\\ \gamma_1 = \beta_2/\beta^* - \sigma_{\omega 2}\kappa^2/\sqrt{\beta^*}. \tag{A.2}$$

F_1 is given by

$$F_1 = \tanh(\arg_1^4), \tag{A.3}$$

$$\arg_1 = \min\left[\max\left(\frac{\sqrt{k}}{0.09\omega y}; \frac{500v}{y^2\omega}\right); \frac{4\rho\sigma_{\omega 2}k}{CD_{k\omega}y^2}\right], \tag{A.4}$$

where y is the distance to the next surface and CD_{kw} is the positive portion of the cross-diffusion term of Eq. (2.6)

$$CD_{k\omega} = \max\left(2\rho\sigma_{\omega 2}\frac{1}{\omega}\frac{\partial k}{\partial x_j}\frac{\partial \omega}{\partial x_j}; 10^{-20}\right). \tag{A.5}$$

And the eddy viscosity is defined as

$$v_t = \frac{a_1 k}{\max(a_1\omega; \Omega F_2)}, \tag{A.6}$$

where Ω is the absolute value of the vorticity. F_2 is given by

$$F_2 = \tanh(\arg_2^2), \tag{A.7}$$

$$\arg_2 = \max\left(\frac{\sqrt{k}}{0.09\omega y}; \frac{500v}{y^2\omega}\right). \tag{A.8}$$

Appendix B. The coefficients of the perturbation weighting function

$$c_i = \frac{z h_e u_i}{2|u_e|}, \tag{B.1}$$

where $z = \coth(Pe) - 1/Pe \approx \min[1, Pe/3]$; Pe is element Peclet number $= (|u_e|h_e)/2v$; u_e is velocity at an element center; u_i is ith component velocity at an element center; h_e is element characteristic length.

References

Arney, M.S., Bai, R., Guevara, E., Joseph, D.D., Liu, K., 1993. Friction factor and holdup studies for lubricated pipelining-I. Experiment and correlations. Int. J. Mult. Flow 19, 1061–1076.

Bai, R., Chen, K., Joseph, D.D., 1992. Lubricated pipelining: stability of core–annular flow. Part 5: experiments and comparison with theory. J. Fluid Mech. 240, 97–142.

Bai, R., Kelkar, K., Joseph, D.D., 1996. Direct simulation of interfacial waves in a high viscosity ratio and axisymmetric core–annular flow. J. Fluid Mech. 327, 1–34.

Bentwich, M., 1964. Two-phase viscous axial flow in a pipe. J. Bas. Engng., 669–672.

Brooks, A.N., Hughes, T.J.R., 1982. Streamline upwind Petrov–Galerkin formulation for convection dominated flows with particular emphasis on the incompressible Navier–Stokes equations. Comput. Meth. Appl. Mech. Engng. 32, 199–259.

Charles, M.E., Govier, G.W., Hodgson, G.W., 1961. The horizontal pipeline flow of equal density of oil–water mixtures. Can. J. Chem. Eng. 39, 17–36.

Charles, M.E., 1963. The pipeline flow of cylindrical forms. Can. J. Chem. Eng. 46.

Choi, H.G., Choi, H., Yoo, J.Y., 1997. A fractional four-step finite element formulation of the unsteady incompressible Navier–Stokes equations using SUPG and linear equal-order element methods. Comput. Meth. Appl. Mech. Engng. 143, 333–348.

Glass, W., 1961. Water addition aids pumping viscous oils. Chem. Eng. Prog. 57, 116.

Huang, A., Christodoulou, C., Joseph, D.D., 1994. Friction fractor and holdup studies for lubricated pipelining-II. Laminar and k–ε models of eccentric core flow. Int. J. Mult. Flow 20, 481–491.

Joseph, D.D., Bai, R., Mata, C., Sury, K., Grant, C., 1998. Self-lubricated transport of bitumen froth. J. Fluid Mech. 386, 127–148.

Laufer, J., 1952. The structure of turbulence in fully developed pipe flow. NACA 1174.

Menter, F.R., 1994. Two equation eddy-viscosity turbulence models for engineering applications. AIAA J. 32 (8), 1598–1605.

Oliemans, R.V.A., Ooms, G., 1986. Core-annular flow of oil and water through a pipeline. In: Hewitt, G.F., Delhaye, J.M., Zuber, N. (Eds.), Multiphase Science and Technology, vol. 2. Hemisphere Publishing Corporation, Washington.

Oliemans, R.V.A., Ooms, G., Wu, H.L., Duÿvestin, A., 1987. Core annular oil/water flow: the turbulent-lubricating-film model and measurements in a 5 cm pipe loop. Int. J. Mult. Flow 13, 22–31.

Oliemans, R.V.A., Ooms, G., Wu, H.L., Duÿvestin, A., 1985. Core-annular flow of oil/water flow: the turbulent-lubricating model and measurements in a 2-in. pipe loop. Presented at the Middle East Oil Technical Conf. and Exhibition, Bahrain, March 11–14, 1985. Soc. Pet. Eng.

Ooms, G., Segal, A., Van der Wees, A.J., Meerhoff, R., Oliemans, R.V.A., Int, J., 1984. A theoretical model for core–annular flow of a very viscous oil core and a water annulus through a horizontal pipe. Int. J. Mult. Flow 10, 41–60.

Patankar, S.V., Liu, C., Sparrow, E.M., 1977. Fully developed flow and heat transfer in ducts having streamwise periodic variations of cross-sectional area. Trans. ASME J. Heat Transfer 99, 180–186.

Patankar, S.V., 1980. Numerical Heat Transfer and Fluid Flow. Hemisphere Publishing Corporation, Washington.

Russell, T.W.F., Charles, M.E., 1959. The effect of the less viscous liquid in the laminar flow of two immiscible liquids. Can. J. Chem. Engng. 39, 18–24.

Russell, T.W.F., Hodgson, G.W., Govier, G.W., 1959. Horizontal pipeline flow of mixtures of oil and water. Can. J. Chem. Eng. 37, 9.

Stein, M.H., 1978. Concentric annular oil/water flow. Ph.D. thesis, Purdue University.